

Deep neural network for Wannier function centers

Linfeng Zhang

*Program in Applied and Computational Mathematics,
Princeton University, Princeton, NJ 08544, USA*

Mohan Chen

CAPT, HEDPS, College of Engineering, Peking University, Beijing 100871, China

Xifan Wu

Department of Physics, Temple University, Philadelphia, PA 19122, USA

Han Wang*

*Laboratory of Computational Physics, Institute of Applied Physics and
Computational Mathematics, Huayuan Road 6, Beijing 100088, China*

Weinan E

*Department of Mathematics and Program in Applied and Computational Mathematics,
Princeton University, Princeton, NJ 08544, USA and
Beijing Institute of Big Data Research, Beijing, 100871, P.R. China*

Roberto Car[†]

*Department of Chemistry, Department of Physics,
Program in Applied and Computational Mathematics,
Princeton Institute for the Science and Technology of Materials,
Princeton University, Princeton, NJ 08544, USA*

We introduce a deep neural network (DNN) model that assigns the position of the centers of the electronic charge in the snapshots of a molecular dynamics trajectory. The electronic centers are uniquely specified by the unitary transformation that maps the occupied eigenstates onto maximally localized Wannier functions. In combination with deep potential molecular dynamics, a DNN approach to model the atomic potential energy surface at the *ab initio* density functional level of theory, the scheme makes possible to predict the dielectric properties of insulators for samples and trajectories inaccessible to direct *ab initio* simulation, without loss of accuracy. As an example, we report calculations of the infrared absorption spectra of light and heavy water at a dispersion inclusive hybrid functional level of theory, finding good agreement with experiment. Extensions to other spectroscopies, like Raman and sum frequency generation, are discussed.

PACS numbers:

In the last decade we have witnessed a large development of machine learning (ML) schemes representing the potential energy surface (PES) of many-atom systems [1–11]. These approaches are trained with first-principle data, typically from electronic density functional theory (DFT) [12], and may boost *ab initio* molecular dynamics (AIMD) [13, 14] by greatly extending the accessible range of the simulations without loss of accuracy. The reduction of statistical errors resulting from larger and longer simulations leads to accurate predictions of static and dynamic properties. In addition, it becomes possible to study rare events, such as, e.g., crystal nucleation, with enhanced sampling methods in simulations of *ab initio* quality [15], instead of relying on numerically efficient, but less accurate, empirical force-fields.

In this context, ML approaches have focused mostly on representing the PES as a function of the nuclear coordinates. Electronic properties, accessible in AIMD, have

only rarely been considered [4, 16–20]. Important examples are the polarization and/or the polarizability needed to model infrared (IR), Raman, and sum frequency generation spectra of insulators. A general formalism for the polarization utilizes maximally localized Wannier functions (MLWFs) [21, 22], i.e. electronic orbitals with minimal spatial spread generated by a unitary transformation of the occupied subspace within DFT. By mapping the electron density onto point charges, located at the centers (WFCs) of the MLWF density distributions, the polarization can be defined as the dipole moment of the system of electronic and nuclear point charges. For finite systems, i.e. molecules or clusters, this is the observable dipole moment, but for infinite periodic systems the dipole moment is defined modulo a quantum [23], and the polarization is not an observable physical property. For both finite and extended systems, however, the polarization correlation functions are physically meaningful

and serve to describe linear response to an external perturbation.

Here we construct a deep neural network (DNN) model to represent the dependence of the WFCs on the molecular environment. The scheme, called deep WFC (DWFC), is an end-to-end model, in the sense that it does not use any *ad hoc* construction to go from the input atomic to the output WFC coordinates. Furthermore, the model is size extensive, preserves the symmetry of the system, and yields a polarization that varies continuously with the atomic coordinates.

In this paper, we specialize to liquid water, where the WFCs can be uniquely associated to the individual molecules, but it would be straightforward to extend the model to systems in which the WFCs can only be associated to atoms. This would be the case when water ions, such as hydronium (H_3O^+) and hydroxide (OH^-), are present in solution (see e.g. Ref. [24]). In these situations, interconversion of neutral molecules and ions accompanies proton transfer events, and the identity of a molecular species in an MD trajectory is not well defined. Yet, the WFCs remain unambiguously associated to the oxygen atoms.

For any insulating atomic configuration the WFCs are specified by a unitary transformation of the ground-state Kohn-Sham orbitals. We focus here on the valence electrons and use pseudopotentials to describe their interaction with the nuclei plus frozen core electrons. As expected from the principle of nearsightedness of the electronic matter [25, 26], we find that in liquid water the WFCs of a molecule depend only on the configuration of that molecule and its neighbors.

We validate the methodology by showing that DWFC and AIMD predict essentially the same molecular dipoles and WFC-atom pair correlations. For spectral calculations we combine DWFC with deep potential molecular dynamics (DPMD), an efficient ML scheme to generate nuclear trajectories of *ab initio* quality [9, 10]. DWFC locates the WFCs in the DPMD snapshots, giving access to the evolution of the polarization and its time correlation functions. We demonstrate this feature by calculating the IR spectra of liquid H_2O and D_2O at a hybrid functional level of theory with greatly reduced statistical errors compared to direct AIMD simulations.

In the DWFC scheme for neat water, we assign 2 hydrogens (H) and 4 WFCs to each oxygen (O) site i . Let $\mathcal{N}_{r_c}^i = \{j, r_{ij} < r_c\}$ be the index set of the atoms j neighboring oxygen i within a cutoff radius r_c . Atom j can be either O or H. Our goal is to construct a map from the coordinates of atoms i and j to 12 numbers, the coordinates of 4 WFCs. The symmetry constraints here are slightly different from those considered for the PES within DPMD [9, 10]. The PES is *invariant* under translation, rotation, and identical particle permutation, while the WFCs are *equivariant*, i.e., they translate and rotate when the atomic positions are trans-

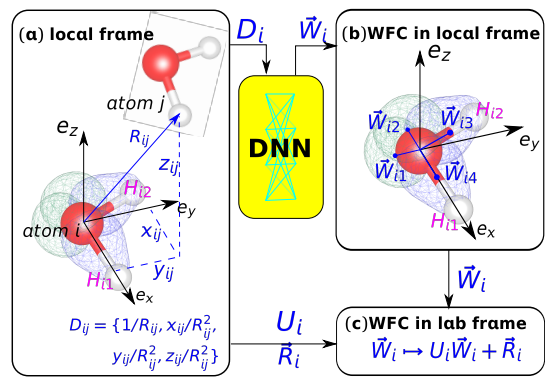


FIG. 1: (Color online) Scheme of the DWFC model for WFCs in liquid water. (a) Local frame and local generalized coordinates. Atom i is a generic oxygen atom and atom $j \in \mathcal{N}_{r_c}^i$ is a generic neighbor of atom i . (e_x, e_y, e_z) defines the local frame of atom i . The oxygen i and the two hydrogens H_{i1} and H_{i2} belong to the same water molecule. We use H_{i1} to denote the hydrogen that is closer to oxygen i . e_x is along the $\text{O}_i\text{-H}_{i1}$ bond. e_z is perpendicular to the plane of the water molecule. e_y is the cross product of e_z and e_x . (e_x, e_y, e_z) forms a local rotation matrix U_i that maps the coordinates of j in the laboratory frame to those in the local frame. (x_{ij}, y_{ij}, z_{ij}) are the Cartesian components of the vector \mathbf{R}_{ij} of length R_{ij} in the local frame. The neural network input $\mathbf{D}_{ij} \equiv \{1/R_{ij}, x_{ij}/R_{ij}^2, y_{ij}/R_{ij}^2, z_{ij}/R_{ij}^2\}$ contains full coordinate information of atom j . We first sort the neighbors of atom i according to their chemical species, e.g. oxygens and then hydrogens. Within each species we sort the atoms in ascending order of distances R_{ij} . \mathbf{D}_i denotes the sorted set of input data for site i . (b) Locations of the 4 WFCs, \mathbf{W}_{ia} ($a = 1, 4$). The DNN takes the set \mathbf{D}_i in input and gives the set $\mathbf{W}_i = \{\mathbf{W}_{ia}, a = 1, 4\}$ in output. The order of the four WFCs is fixed in the local frame. (c) Using the coordinates of site i and the rotation matrix U_i , the coordinates of the WFCs are transformed to the laboratory frame.

lated and rotated, guaranteeing a continuous evolution of the molecular dipoles. For this purpose we associate a local frame to each oxygen atom, O_i . In the local frame we sort the set $\mathcal{N}_{r_c}^i$ in ascending order of distance from O_i and specify a corresponding order for the WFCs. As shown in Fig. 1, the i -th local frame is defined by oxygen O_i and its two nearest hydrogens, H_{i1} and H_{i2} . The ordered local coordinate information is encoded in $\mathbf{D}_{ij} = \{1/R_{ij}, x_{ij}/R_{ij}^2, y_{ij}/R_{ij}^2, z_{ij}/R_{ij}^2\}$, wherein $x_{ij} = x_j - x_i$, $y_{ij} = y_j - y_i$, $z_{ij} = z_j - z_i$, in terms of the Cartesian coordinates of atoms i and j in the local frame, $R_{ij} = \sqrt{x_{ij}^2 + y_{ij}^2 + z_{ij}^2}$, and the factor $1/R_{ij}$ reduces the weight of the more distant atoms. The set $\mathbf{D}_i \equiv \{\mathbf{D}_{ij}, j \in \mathcal{N}_{r_c}^i\}$ is the input of a DNN, which returns 12 numbers in output through multiple hidden layers, in each one of which the data undergo a linear transformation followed by the action of a non-linear activation function. In the final step

from the last hidden layer to the ordered WFC positions $\mathbf{W}_i = \{\mathbf{W}_{i1}, \mathbf{W}_{i2}, \mathbf{W}_{i3}, \mathbf{W}_{i4}\}$, only the linear transformation is applied. We call f^γ the map $\mathbf{D}_i \mapsto \mathbf{W}_i$, where γ are the parameters of the linear transformations. We use the hyperbolic tangent for the activation function and adopt 4 hidden layers with decreasing number of nodes, i.e., 200, 100, 50, and 20 nodes, respectively, from the innermost to the outermost layer.

To apply our protocol we first identify and then order equivariantly the four WFCs associated to O_i . The first task is accomplished by selecting the WFCs whose distance from O_i is less than 0.8 Å. The second task is accomplished by identifying $\{\mathbf{W}_{i1}, \mathbf{W}_{i2}, \mathbf{W}_{i3}, \mathbf{W}_{i4}\}$ as in Fig. 1 (b). In the local frame, \mathbf{W}_{i1} and \mathbf{W}_{i2} lie approximately along the \mathbf{e}_z axis perpendicular to the molecular plane of O_i , H_{i1} , and H_{i2} . \mathbf{W}_{i1} and \mathbf{W}_{i2} are lone pair centers. \mathbf{W}_{i3} and \mathbf{W}_{i4} , which lie approximately along the two bonding O-H directions, are bond pair centers. To establish a unique order we assign \mathbf{W}_{i1} (\mathbf{W}_{i2}) to the positive (negative) \mathbf{e}_z direction, and assign \mathbf{W}_{i3} (\mathbf{W}_{i4}) to the $\text{O}_i\text{-H}_{i1}$ ($\text{O}_i\text{-H}_{i2}$) bond. In this way f^γ is a well-defined one-to-one map in the i -th environment. The parameters γ are determined by training, i.e., an optimization process that minimizes a loss function, which is here the mean square difference between the DWFC prediction and the training data. The Adam stochastic gradient descent method [27] is adopted for the optimization.

To construct the DPMD and DWFC models for liquid water, we used data from a path-integral (PI) AIMD simulation of 64 H_2O molecules with periodic boundary conditions [28]. The electronic structure within DFT was calculated with the dispersion inclusive hybrid functional PBE0-TS [29, 30] as in Ref. [31]. The training data were taken from an equilibrated PI-AIMD trajectory lasting 8 ps at isothermal-isobaric conditions with $P = 1$ bar and $T = 300$ K. The calculated equilibrium density was 1.01 g/cm³ (1.00 g/cm³ in experiment). The integration of the equations of motion for the Feynman paths used the i-PI code [32] interfaced with the CP module of Quantum Espresso [33, 34] to compute on the fly the Born-Oppenheimer ground-state of the electrons. The i-PI code used 8 beads to sample the Feynman paths with the generalized Langevin equation [35]. DPMD training was made with the DeePMD-kit [36] using the smooth version of the model [11] to eliminate the small discontinuities associated to sharp cutoff and permutations in the original model [10]. The smooth version makes possible to generate the long microcanonical trajectories needed to evaluate classical time correlation functions with small statistical errors.

To train the DWFC model we used 90% of the snapshots from the PI-AIMD trajectory, leaving the rest for testing. In addition, we used DWFC to predict the WFC evolution along an independent classical AIMD trajectory (with the same DFT approximation) at $T = 330$ K

and a simulation box fixed at the experimental density at room temperature [31]. In our model the only adjustable parameter is the cutoff radius r_c . We found that the error decreases with increasing r_c and converges to a small finite value when r_c is large enough to include the first shell of neighboring molecules. With our adopted choice, i.e. $r_c = 4.5$ Å, the root mean square error (RMSE) in the predicted WFC positions is 0.0033 (0.0049) Å in our classical (PI) AIMD trajectories. As in Ref. [37] we define the dipole moment of the i -th molecule in terms of the atom and WFC positions in the laboratory frame by $\boldsymbol{\mu}_i = e(6\mathbf{R}_{\text{O}_i} + \mathbf{R}_{\text{H}_{i1}} + \mathbf{R}_{\text{H}_{i2}} - 2\sum_{a=1}^4 \mathbf{R}_{\text{W}_{ia}})$, where e denotes the electronic charge. The RMSE of the predicted dipole moments is 0.032 (0.038) Debye, approximately 1% of the average value, in the classical (PI) trajectories. Since only PI-AIMD trajectories were used for training, the good performance for the classical trajectory at $T = 330$ K indicates some transferability of the model to different thermodynamic conditions.

Next, we use DWFC to access the WFC evolution over long DPMD trajectories. We report in Fig. 2 the atom-WFC and dipole distributions for quantal (PI-DPMD) and classical (DPMD) 1-ns-long trajectories, at the thermodynamic conditions used to train and test the DWFC model. A comparison with two corresponding, but much shorter, AIMD trajectories shows excellent agreement in the calculated WFC distributions.

Finally, we illustrate the usefulness of the DPMD+DWFC scheme by calculating the IR absorption spectra of liquid H_2O and D_2O for a cell with 512 molecules under periodic boundary conditions. We use two microcanonical trajectories lasting 500 ps each, for H_2O and D_2O , corresponding to an average temperature of ~ 300 K at the equilibrium density of the PI-AIMD simulation at $T = 300$ K. The frequency dependent absorption coefficient per unit length, $\alpha(\omega)$, is given by the Fourier transform of the time correlation function of the polarization $\mathbf{M} = \sum_i \boldsymbol{\mu}_i$, according to:

$$\alpha(\omega) = \frac{2\pi\omega^2\beta}{3cVn(\omega)} \int_{-\infty}^{+\infty} dt e^{-i\omega t} \langle \mathbf{M}(0) \cdot \mathbf{M}(t) \rangle, \quad (1)$$

where $n(\omega)$ is the refractive index, which is a constant taken from experiment within the relevant frequency range, V is the volume, $\beta = 1/k_B T$ is the inverse temperature, and k_B is the Boltzmann factor. The calculated spectra are reported in Fig. 3 together with the corresponding experimental observations. As a further check, we calculated the variance of the spectra predicted by DNN models that differ among themselves only in the initialization of the network parameters γ . Due to the highly non-linear dependence of f^γ on γ , different initializations result in multiple local minima in the landscape of the loss function, originating an ensemble of minimizing DNNs. The variance of the predictions within this ensemble is an intrinsic property of a DNN model and

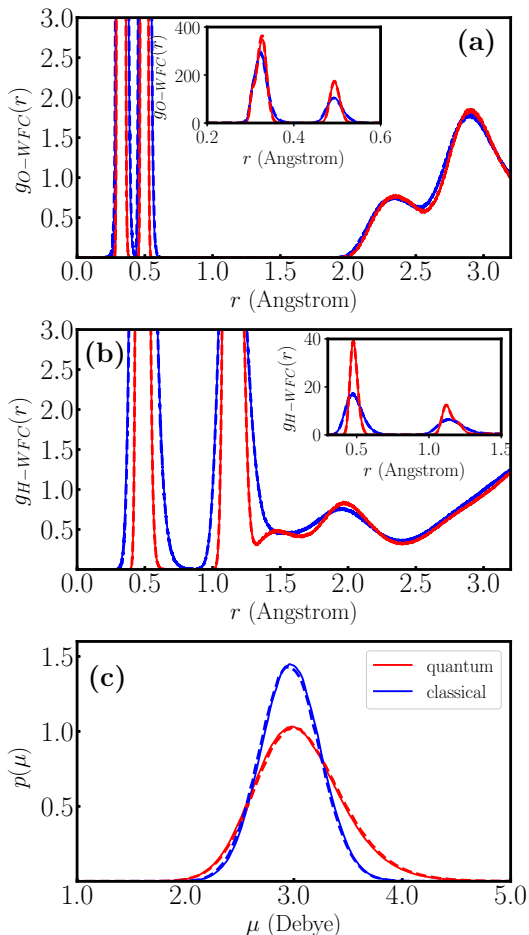


FIG. 2: (Color online) Distribution functions associated to the WFCs on quantum, i.e., PI, (red) and classical (blue) trajectories: (a) O-WFC pair correlation function $g_{O-WFC}(r)$; (b) H-WFC pair correlation function $g_{H-WFC}(r)$; (c) probability distribution of the magnitude for the molecular dipole (μ). Solid (dashed) lines refer to DWFC (AIMD) (see text).

can be used as an indicator of its accuracy [16, 40–42]. Using this criterion and a normally distributed random choice of initial parameters, we obtain a relative variance uniformly smaller than 1%, i.e., smaller than the line width of the spectra in Fig. 3.

Overall, the agreement of theory and experiment is good. The spectra are characterized by 4 main features, i.e., in order of decreasing frequencies, OH stretching, molecular bending, molecular libration, and hydrogen bond network modes (see, e.g., Ref. [37]). The calculated H_2O spectrum is blue-shifted by $\sim 45 \text{ cm}^{-1}$ relative to experiment in the stretching region. The corresponding shift is barely noticeable in D_2O . Relative to experiment, the theoretical spectra of H_2O and D_2O exhibit sharper bending peaks and more intense, blue shifted, far IR features.

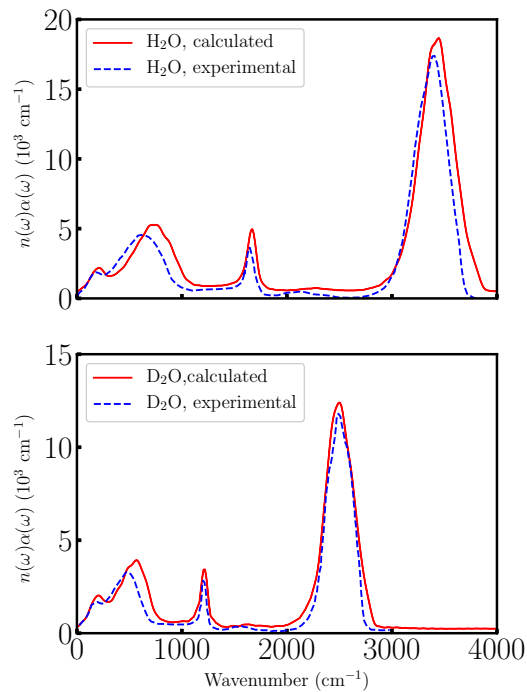


FIG. 3: (Color online) IR absorption spectra of H_2O (upper panel) and D_2O (lower panel). The continuous lines report DPMD+DWFC calculations (512 molecules, 0.5 ns trajectories). The variance of the spectra estimated from the DNN ensemble (see text) is smaller than the line width. The dashed lines report experimental data for H_2O at 298 K (Ref. [38]) and for D_2O at 295 K (Ref. [39]).

The small differences between theory and experiment should be attributed to the adopted DFT approximation and the use of a classical instead of a quantum auto-correlation function in Eq. 1. Ref. [43] showed that the hybrid functional PBE0 yields a substantially better IR spectrum than semilocal functionals like PBE [44]. Our simulation used PBE0 with dispersion corrections for a better description of the liquid structure [31]. Quantum fluctuations affect static and dynamic response of water, but while static correlations can be evaluated without approximation with path integral simulations, dynamic correlations require integrals of complex functions, whose evaluation is a major challenge for statistical simulation methods. Recently, quantum IR correlations have been calculated for water using approximate methods like ring polymer [45] and centroid [45, 46] MD, indicating that quantum corrections tend to red shift the classical spectral features. Further studies of these issues will be facilitated by methods like DPMD and DWFC, which greatly improve the statistical quality of *ab initio* simulations.

In summary, DWFC is a powerful tool to parametrize

the dependence of the electronic charge centers on the atomic environment. Our approach could be extended to deal with other electronic properties, such as, e.g., the molecular polarizability tensors $\alpha_{\delta\sigma}^i = \frac{\partial \mu_{i\delta}}{\partial E_\sigma}$, where $\mu_{i\delta}$ is the δ -Cartesian component of the dipole $\boldsymbol{\mu}_i$ and E_σ is the σ -component of a uniform electric field. A DNN could be constructed to represent the dependence of $\alpha_{\delta\sigma}^i$ on the i -th molecular environment $\{\mathbf{R}_i, \mathbf{R}_j, j \in \mathcal{N}_{r_c}^i\}$ specified by a cutoff radius r_c , like what we have done for the WFCs. In this way we could compute Raman [47] and sum frequency generation spectra [48, 49]. Access to the combined evolution of the nuclear coordinates and the associated polarization in simulations of large systems over long time scales should also open the way to MD studies of ferroelectric phase transitions without relying on effective Hamiltonian models [50–52]. Finally, we recall that most ML schemes [1, 2, 8, 11], including DPMD, represent the PES by a sum of atomic terms $E_i(\{\mathbf{R}_i, \mathbf{R}_j, j \in \mathcal{N}_{r_c}^i\})$, which are short ranged in spite of being trained with AIMD data that contain long range electrostatics. Explicit inclusion of long range electrostatic effects in DPMD may be necessary to describe properties like the longitudinal-transverse splitting of the optical phonons in ionic materials. In these situations, the DWFC scheme could be used to define a PES representation that includes explicitly the electrostatic energy of the system of nuclear and electronic point charges.

The work of L. Z., X. W., W. E, and R.C. was conducted at the Center “Chemistry in Solution and at Interfaces” (CSI) funded by the DOE Award DE-SC001934. The work of L. Z and W. E was partially supported by a gift from iFlytek to Princeton University and by ONR grant N00014-13-1-0338. The work of H.W. was supported by the NSFC under grant 11871110, and the National Key Research and Development Program of China under grants 2016YFB0201200 and 2016YFB0201203. We are grateful for computing time at the Terascale Infrastructure for Groundbreaking Research in Science and Engineering (TIGRESS) of Princeton University.

* Electronic address: wang_han@iapcm.ac.cn

† Electronic address: rcar@princeton.edu

- [1] J. Behler and M. Parrinello, *Physical Review Letters* **98**, 146401 (2007).
- [2] A. P. Bartók, M. C. Payne, R. Kondor, and G. Csányi, *Physical Review Letters* **104**, 136403 (2010).
- [3] M. Rupp, A. Tkatchenko, K.-R. Müller, and O. A. VonLilienfeld, *Physical Review Letters* **108**, 058301 (2012).
- [4] G. Montavon, M. Rupp, V. Gobre, A. Vazquez-Mayagoitia, K. Hansen, A. Tkatchenko, K.-R. Müller, and O. A. Von Lilienfeld, *New Journal of Physics* **15**, 095003 (2013).
- [5] V. Botu, R. Batra, J. Chapman, and R. Ramprasad, *The Journal of Physical Chemistry C* **121**, 511 (2016).
- [6] S. Chmiela, A. Tkatchenko, H. E. Sauceda, I. Poltavsky, K. T. Schütt, and K.-R. Müller, *Science Advances* **3**, e1603015 (2017).
- [7] K. Schütt, P.-J. Kindermans, H. E. S. Felix, S. Chmiela, A. Tkatchenko, and K.-R. Müller, in *Advances in Neural Information Processing Systems* (2017) pp. 992–1002.
- [8] J. S. Smith, O. Isayev, and A. E. Roitberg, *Chemical Science* **8**, 3192 (2017).
- [9] J. Han, L. Zhang, R. Car, and W. E, *Communications in Computational Physics* **23**, 629 (2018).
- [10] L. Zhang, J. Han, H. Wang, R. Car, and W. E, *Physical Review Letters* **120**, 143001 (2018).
- [11] L. Zhang, J. Han, H. Wang, W. Saidi, R. Car, and W. E, in *Advances in Neural Information Processing Systems 31*, edited by S. Bengio, H. Wallach, H. Larochelle, K. Grauman, N. Cesa-Bianchi, and R. Garnett (Curran Associates, Inc., 2018) pp. 4441–4451.
- [12] W. Kohn and L. J. Sham, *Physical Review* **140**, A1133 (1965).
- [13] R. Car and M. Parrinello, *Physical Review Letters* **55**, 2471 (1985).
- [14] D. Marx and J. Hutter, *Ab initio molecular dynamics: basic theory and advanced methods* (Cambridge University Press, 2009).
- [15] L. Bonati and M. Parrinello, *Physical Review Letters* **121**, 265701 (2018).
- [16] M. Gastegger, J. Behler, and P. Marquetand, *Chemical Science* **8**, 6924 (2017).
- [17] A. Grisafi, D. M. Wilkins, G. Csányi, and M. Ceriotti, *Physical Review Letters* **120**, 036002 (2018).
- [18] A. Grisafi, A. Fabrizio, B. Meyer, D. M. Wilkins, C. Corminboeuf, and M. Ceriotti, *ACS Central Science* **5**, 57 (2018).
- [19] D. M. Wilkins, A. Grisafi, Y. Yang, K. U. Lao, R. A. DiStasio, and M. Ceriotti, *Proceedings of the National Academy of Sciences*, 201816132 (2019).
- [20] A. Chandrasekaran, D. Kamal, R. Batra, C. Kim, L. Chen, and R. Ramprasad, *NPJ Computational Materials* **5**, 22 (2019).
- [21] N. Marzari and D. Vanderbilt, *Physical Review B* **56**, 12847 (1997).
- [22] N. Marzari, A. A. Mostofi, J. R. Yates, I. Souza, and D. Vanderbilt, *Reviews of Modern Physics* **84**, 1419 (2012).
- [23] R. Resta, *Reviews of Modern Physics* **66**, 899 (1994).
- [24] M. Chen, L. Zheng, B. Santra, H.-Y. Ko, R. A. DiStasio Jr, M. L. Klein, R. Car, and X. Wu, *Nature Chemistry*, 1 (2018).
- [25] W. Kohn, *Physical Review Letters* **76**, 3168 (1996).
- [26] E. Prodan and W. Kohn, *Proceedings of the National Academy of Sciences* **102**, 11635 (2005).
- [27] D. Kingma and J. Ba, in *Proceedings of the International Conference on Learning Representations (ICLR)* (2015).
- [28] B. Santra, H.-Y. Ko, L. Zhang, R. A. DiStasio Jr., and R. Car, “Nuclear Quantum Effects in Liquid Water and Ice,” (in prep.).
- [29] C. Adamo and V. Barone, *The Journal of Chemical Physics* **110**, 6158 (1999).
- [30] A. Tkatchenko and M. Scheffler, *Physical Review Letters* **102**, 073005 (2009).
- [31] R. A. DiStasio Jr, B. Santra, Z. Li, X. Wu, and R. Car, *The Journal of Chemical Physics* **141**, 084502 (2014).
- [32] M. Ceriotti, J. More, and D. E. Manolopoulos, *Computer Physics Communications* **185**, 1019 (2014).

- [33] P. Giannozzi, S. Baroni, N. Bonini, M. Calandra, R. Car, C. Cavazzoni, D. Ceresoli, G. L. Chiarotti, M. Cococcioni, I. Dabo, A. Dal Corso, S. de Gironcoli, S. Fabris, G. Fratesi, R. Gebauer, U. Gerstmann, C. Gougoussis, A. Kokalj, M. Lazzeri, L. Martin-Samos, N. Marzari, F. Mauri, R. Mazzarello, S. Paolini, A. Pasquarello, L. Paulatto, C. Sbraccia, S. Scandolo, G. Sclauzero, A. P. Seitsonen, A. Smogunov, P. Umari, and R. M. Wentzcovitch, *Journal of Physics: Condensed Matter* **21**, 395502 (2009).
- [34] P. Giannozzi, O. Andreussi, T. Brumme, O. Bunau, M. B. Nardelli, M. Calandra, R. Car, C. Cavazzoni, D. Ceresoli, M. Cococcioni, N. Colonna, I. Carnimeo, A. D. Corso, S. d. Gironcoli, P. Delugas, R. A. DiStasio Jr., A. Ferretti, A. Floris, G. Fratesi, G. Fugallo, R. Gebauer, U. Gerstmann, F. Giustino, T. Gorni, J. Jia, M. Kawamura, H.-Y. Ko, A. Kokalj, E. Küçükbenli, M. Lazzeri, M. Marsili, N. Marzari, F. Mauri, N. L. Nguyen, H.-V. Nguyen, A. Otero-de-la Roza, L. Paulatto, S. Poncé, D. Rocca, R. Sabatini, B. Santra, M. Schlipf, A. P. Seitsonen, A. Smogunov, I. Timrov, T. Thonhauser, P. Umari, N. Vast, X. Wu, and S. Baroni, *Journal of Physics: Condensed Matter* **29**, 465901 (2017).
- [35] M. Ceriotti, D. E. Manolopoulos, and M. Parrinello, *The Journal of Chemical Physics* **134**, 084104 (2011).
- [36] H. Wang, L. Zhang, J. Han, and W. E, *Computer Physics Communications* **228**, 178 (2018).
- [37] W. Chen, M. Sharma, R. Resta, G. Galli, and R. Car, *Physical Review B* **77**, 245114 (2008).
- [38] J. E. Bertie and Z. Lan, *Applied Spectroscopy* **50**, 1047 (1996).
- [39] J. E. Bertie, M. K. Ahmed, and H. H. Eysel, *The Journal of Physical Chemistry* **93**, 2210 (1989).
- [40] J. S. Smith, B. Nebgen, N. Lubbers, O. Isayev, and A. E. Roitberg, *The Journal of Chemical Physics* **148**, 241733 (2018).
- [41] L. Zhang, H. Wang, and W. E, *The Journal of Chemical Physics* **148**, 124113 (2018).
- [42] L. Zhang, D.-Y. Lin, H. Wang, R. Car, and W. E, *Physical Review Materials* **3**, 023804 (2019).
- [43] C. Zhang, D. Donadio, F. Gygi, and G. Galli, *Journal of Chemical Theory and Computation* **7**, 1443 (2011).
- [44] J. P. Perdew, K. Burke, and M. Ernzerhof, *Physical Review Letters* **77**, 3865 (1996).
- [45] O. Marsalek and T. E. Markland, *The Journal of Physical Chemistry Letters* **8**, 1545 (2017).
- [46] G. R. Medders and F. Paesani, *Journal of Chemical Theory and Computation* **11**, 1145 (2015).
- [47] Q. Wan, L. Spanu, G. A. Galli, and F. Gygi, *Journal of Chemical Theory and Computation* **9**, 4124 (2013).
- [48] S. Mukamel, *Principles of nonlinear optical spectroscopy*, Vol. 41 (1998) pp. 591–592.
- [49] Y. Nagata and S. Mukamel, *Journal of the American Chemical Society* **132**, 6434 (2010).
- [50] R. Resta and D. Vanderbilt, in *Physics of Ferroelectrics* (Springer, 2007) pp. 31–68.
- [51] V. Srinivasan, R. Gebauer, R. Resta, and R. Car, in *AIP Conference Proceedings*, Vol. 677 (AIP, 2003) pp. 168–175.
- [52] D. Vanderbilt and W. Zhong, *Ferroelectrics* **206**, 181 (1998).